Lipid nanocapsules as *in vivo* oxygen sensors using magnetic resonance imaging

Janske Nel[a,b], Florence Franconi[a,c], Nicolas Joudiou[b,d], Patrick Saulnier[a], Bernard Gallez[b], Laurent Lemaire[a,c,*]

[a] Micro et Nanomedecines translationnelles, MINT, UNIV Angers, INSERM 1066, CNRS 6021, 4 rue Larrey, Angers, France
[b] Biomedical Magnetic Resonance Unit (REMA), Louvain Drug Research Institute, Université Catholique de Louvain, Avenue Mounier 73 bte B1.73.08, 1200 Brussels, Belgium
[c] PRISM, UNIV d'Angers, 4 rue Larrey, Angers F-49933, France
[d] Nuclear and Electron Spin Technologies Platform (NEST), Louvain Drug Research Institute, Université Catholique de Louvain, Avenue Mounier 73 bte B1.73.08, 1200 Brussels, Belgium

ARTICLE INFO

ABSTRACT

Hypoxia is common occurrence of the tumour microenvironment, wherein heterogeneous gradients of O_2 give rise to tumoural cells which are highly malignant, metastatic, and resistant to therapeutic efforts. Thus, the assessment and imaging of hypoxia is essential for tumour diagnosis and treatment. Magnetic resonance imaging and, more specifically, the quantitative assessment of longitudinal relaxation time enhancement, was shown to enable the mapping of oxygen in tumours with increased sensitivity for lipids as compared to water signal. Unfortunately, this can only be applied to tumours with high lipid content. To overcome this issue, we propose the use of lipid nanocapsules (LNCs). LNCs have been demonstrated as excellent core-shell nanocarriers, wherein the lipidic-core is used for lipophilic drug encapsulation, enabling treatment of highly malignant tumours. Herein, however, we exploited the lipidic-core of the LNCs to develop a simple but effective technique to increase the lipidic content within tissues to enable the assessment and mapping of pO_2. LNCs were prepared using the phase-inversion technique to produce 60 nm sized nanoparticles, and *in vitro* studies demonstrated the permeability and responsiveness of LNCs to O_2. To evaluate the ability of LNCs to respond to changes in pO_2 *in vivo*, after a hyperoxic challenge, three animal models, namely a normal tissue model (gastrocnemius muscle tissue) and two tumour tissue models (subcutaneous fibrosarcoma and intracerebral glioblastoma) were explored. LNCs were found to be responsive to variation of O_2 *in vivo*. Moreover, the use of MRI enabled the mapping of oxygen gradients and heterogeneity within tumours.

1. Introduction

Hypoxia is a key feature in solid tumours caused by abnormal and torturous vasculature which are unable to meet the O_2 demand of the tumour mass. This oxygen deprivation causes; a change in gene expression; leading to more aggressive tumours; and results in metastatic progression and resistance to radiation and chemotherapy [1,2]. Thus, a need has risen to combat the poor outcome of treatment interventions by developing techniques to image and assess the hypoxic tumour environment. Ideally, the imaging of hypoxia should be non-invasive, sensitive, robust, quantitative, widely available and able to reflect tumour heterogeneity. To this end, techniques such as electron paramagnetic resonance and positron emission tomography imaging have been developed, but magnetic resonance imaging (MRI) techniques are more appealing due to its ability to provide spatial information and its use of non-ionising probes.

The development of perfluorinated compounds began the use of ^{19}F-based MR oximetry and introduced the use of exogenous probes [3–5],

however their *in vivo* application was limited by the need for specialist MR equipment regarding the ^{19}F-tuned probe. Endogenous probes, such as water and lipids, had no such limitation. Regardless the origin of the sensor, oxygen measurement is based on the change in longitudinal relaxation time (T_1). Indeed, molecular oxygen (O_2) possesses two unpaired electrons which enable its paramagnetic ability to act as a T_1-shortening agent in tissues [6], and therefore as a signal intensity enhancer on MR T_1-weighted sequences [7]. Therefore, the change of oxygenation is also directly correlated with the longitudinal relation rate ($1 / T_1 = R_1$) [4,8]. Despite being attractive for oxygenation measurements, with respect to the high water content of biological tissues, water T_1 change with oxygen concentration is limited, and lower than the change observed with lipids, due the six times higher solubility of oxygen in lipids than in water [9]. This property was exploited by Jordan and colleagues who developed an MR sequence to map oxygen based on imaging of lipid relaxation rates (MOBILE; acronym for mapping of oxygen my imaging of lipid relaxation enhancement) [10].

The drawback of this method however, is that there is not always a sufficient amount of intrinsic lipids in the tissue of interest to enable the use of the MOBILE method. This limitation can be overcome by the use of lipid nanocapsules (LNCs) [11]: a nanocarrier with an oil-filled core surrounded by a protective polymer shell, capable of encapsulating drugs, with proven treatment efficiency in preclinical glioblastoma cancer models [12–14]. Thus, while delivering therapy, an increase in lipid level can be reached allowing MR oxygenation mapping using the described MOBILE method. Notably, LNCs are also of particular interest due to their O_2 permeability [15], solvent free and FDA-approved constituents, and their ability to avoid the immune system [16]. Using the MOBILE MR sequence, LNCs were investigated for their ability to respond to changes in O_2 concentrations *in vitro*. For *in vivo* experiments, a muscle model and two tumour models were employed to assess the ability of the LNCs to act as an oxygen sensor during carbogen respiratory challenges.

2. Materials and methods

2.1. Reagents

The lipophilic Labrafac® WL 1349 (caprylic-capric acid triglycerides; European Pharmacopeia, IVth, 2002) was purchased from Gattefossé S.A. (Saint-Priest, France). Lipoïd S75-3 (soybean lecithin at 69% of phosphatidylcholine) and Kolliphor® HS 15 (a mixture of free polyethylene glycol 660 and polyethylene glycol 660 hydroxystearate) were provided by Lipoïd GmbH (Ludwigshafen, Germany) and BASF (Ludwigshafen, Germany), respectively. NaCl was purchased from Prolabo (Fontenay-sous-Bois, France). Filtered and deionised water was obtained from a Milli-Q plus® system (Millipore).

2.2. Formulation and characterisation of LNCs

LNCs were prepared according to the phase inversion method [11]. Briefly, 1.028 g of Labrafac (oil phase), Lipoïd (0.075 g), Kolliphor® HS 15 (0.846 g), NaCl (0.148 g) and water (2.962 g) were mixed and heated to 95 °C with magnetic stirring. Thereafter the mixture underwent three cycles of cooling and heating between 50 °C and 95 °C. After the final heating phase, the solution was cooled to 72 °C and subjected to an irreversible shock induced by adding 1 mL of 4 °C water. This fast cooling allowed for the formation of stable, core-shell LNCs. Thereafter, the osmolarity of the formulation was adjusted to be physiologically safe for *in vivo* administration. To achieve this, 1 mL of the LNC formulation was dialysed using dialysis tubing (Spectra Biotech Cellulose Ester Dialysis Membrane, MWCO = 100 kDa) for 24 h against pure water (Milli-Q plus® system, Millipore), changing the water hourly for 6 h. Then, to obtain the original volume of LNCs, the dilution factor of the dialysed solution was calculated and evaporation, using N_2, with magnetic stirring was done. Once the initial volume was obtained,

evaporation was ceased and 30 μL of a salt solution (320 mg/mL) was added. Osmolarity measurements were performed using a 5520 Vapro vapour osmometer from Wescor (Logan, Utah, USA). Osmolarity adjusted LNCs were used for all *in vivo* experiments. The average hydrodynamic size and polydispersity index (PDI) of the LNCs were determined by dynamic light scattering using a Malvern Zetasizer® (Nano Series DTS 1060, Malvern Instruments S.A., Worcestershire, UK) fitted with a 633 nm laser beam (helium–neon laser, 4 mW) at a fixed scattered angle of 173°. To ensure accuracy, LNCs were diluted 1:60 (v/v) in deionised water to produce scattering intensity values that were in the midrange of the instrument's detector. Values are expressed as mean of three measurements ± standard deviation (SD) for five formulations.

2.3. In vitro sensitivity of LNCs to pO2

To evaluate the response of LNCs to variations in O_2, the MOBILE sequence was applied wherein the T_1 of the methylene group (~1.2 ppm) of the lipid core of the LNCs was measured at 37 °C in sealed tubes bubbled with nitrogen (0% O_2), air (21% O_2) or pure oxygen (100% O_2) for 30 min with magnetic stirring. Temperature of the samples was maintained using a warm water circulation system. MOBILE sequence acquisition parameters were as follows; repetition time (TR): 1520 ms; mean echo time (TE): 0.8 ms, flip angle: 5°; bandwidth (BW): 200 kHz at 30% echo position; matrix: 32 × 32, field of view (FOV): 5 × 5 cm; 16 segments, a series of 50 images spaced at TR 29.80 ms with a slice thickness of 4 mm, and a total acquisition time of approximately 35 min. Determination and acquisition of the lipid signal was adapted from Jordan et al. [10]. Briefly, the difference in frequency between the water and lipid peaks (*i.e.* 1.2 ppm for the methylene group of the lipid core of LNCs) in a ^{1}H proton spectrum was determined and used as the offset for the imaging frequency for the MOBILE sequence. A Gaussian saturation pulse of 2.74 ms with a 1000 Hz frequency range to spoil the water signal was applied.

2.4. Animal model care and preparation

Animal care and use were in accordance with the regulations of the French Ministry of Agriculture and approved by the Pays de la Loire Ethics in Animal Experimentation Committee under project number 01858.03. Animals were housed in a controlled and pathogen-free environment, with free access to food and water, at the University animal facility (SCAHU-Angers, France). Animal anaesthesia was induced by a continuous flow of air (0.5–0.8 L/min) and 3% isoflurane (Piramal Healthcare, UK Limited, Northumberland, UK) and maintained with 0.5–1% isoflurane. Body temperature was maintained during MR acquisition using a heated water circulating system. Respiration was also monitored. Three animal models were used in this *in vivo* study; an intramuscular tissue model and two tumoural tissue models, namely subcutaneous fibrosarcoma and intracerebral glioblastoma tumours.

2.4.1. Normal gastrocnemius muscle animal model
Five 7-week old male C3H/HeJ mice (Janvier, Le Genest-Saint-Isle, France) were used for the intramuscular tissue study.

2.4.2. Cell culture for tumoural animal models
Two tumour models were used in this study; a subcutaneous fibrosarcoma model and an intracerebral glioblastoma model. Culture reagents were obtained from Thermo Fisher Scientific, Gibco and BioWhittaker (France). For the subcutaneous fibrosarcoma model, the syngenic FSaII fibrosarcoma murine cell line [17] was utilised and grown in Dulbecco's modified Eagle's medium (DMEM) high glucose GlutaMAX supplemented with 10% bovine serum and 1% Pen/Strep. For the intracerebral glioblastoma model, the C6 rat glioma cell line was purchased from ECACC and was grown in Ham's F12 medium, supplemented with 1 mM L-glutamine, 10% bovine serum and 1% Pen/Strep. Cells were grown in standard cell culture conditions (21% O_2, 5%

CO$_2$ and 37 °C).

2.4.2.1. *Subcutaneous fibrosarcoma tumour model.* Seven male 7-week-old C3H/HeJ mice (Janvier, Le Genest-Saint-Isle, France) were inoculated subcutaneously into the hind thigh with 2×10^6 FSaII cells in 100 μL serum-free DMEM under isoflurane anaesthesia. MR experiments were undertaken once tumours reached 8–10 mm in diameter.

2.4.2.2. *Intracerebral glioblastoma tumour model.* Glioblastomas were induced in the caudate putamen of 10–12 week-old female Sprague-Dawley rats (n = 6) (SCAHU-Angers, France) *via* the stereotaxic inoculation of C6 rat glioma cells as previously described [18]. Briefly, under Rompun® (Xylazine, Bayer AG, Leverkusen, Germany) and Clorketam® (Kétamine, Vétoquinol, Lure, France) anaesthesia, rats were fixed in a stereotaxic holder and placed on a heating pad to maintain the appropriate physiological temperature. Through a 1 mm drilled hole in the skull (anterior 5 mm, lateral 3 mm, depth 7 mm in respect to bregma), a 5 μL suspension of 4.0×10^4 C6 rat glioma cells were injected over a 10 min period into the caudate putamen of the right hemisphere. After surgery, rats received a single 30 μg/kg subcutaneous injection of Vetergesic® (buprenorphine, Sogeval, France) for pain management. Animals were monitored daily for grooming and mobility, and MR experiments commenced when tumours reached approximately 30 μL in volume.

2.5. *MR experiments*

MR imaging was performed using a 7 T scanner (Biospec 70/20 Avance III, Bruker Wissembourg, France) equipped with BGA12S gradient system (675 mT/m). Emission was ensured by an 86 mm diameter resonator and reception by a 2×2 surface array coil positioned over the rat head for C6-glioma experiment and or a 2 cm diameter loop coil positioned under the mouse leg or tumour. For the duration of all MR experiments, animal temperature was regulated by a heated water-circulating system. For anatomical images, T$_2$-weighted rapid acquisition with refocused echoes (RARE) set of images was acquired to follow the volume of tumours (TR = 3200 ms; TE = 21.3 ms; RARE factor = 4; FOV = 4×4 cm; matrix = 256×256; nine contiguous slices of 0.5 mm, Nex = 1). Thus, once tumours were of proper size, the LNC suspension was injected into the tissue. Animals were anaesthetised, and a bolus injection of 40 μL was injected intramuscularly in the normal tissue model, or intratumourally for the subcutaneous fibrosarcoma tumour model. For LNC delivery into the intracerebral glioblastoma tumour model, a convection-enhanced delivery (CED) protocol [19,20] was implemented to provide a well-diffused distribution of the 40 μL LNCs in the brain tumour. Once the LNC suspension was introduced into the animal model, T$_1$ was measured using the MOBILE MR sequence (with acquisition parameters described in Section 2.3, with geometry changes for *in vivo* experiments adjusted as follows; slice of 3 mm, and a FOV = 1×1 cm for mice and 3×3 cm for rats). LNC T$_1$ sensitivity to oxygen variation in the different animal models was assessed using a carbogen (95% O$_2$, 5% CO$_2$) breathing challenge [7].

2.5.1. *T$_1$ lipid measurement using MOBILE*

The MOBILE sequence, described by Jordan et al. [10] as a segmented inversion-recovery fast imaging with steady state precession (IR FISP), was used to acquire images in order to calculate T$_1$ relaxation time maps while the animal was breathing air and carbogen. After the acquisition of the T$_1$-weighted MOBILE MR image set, the T$_1$ was calculated using a non-linear fit with a home-made program written in Matlab (The MathWorks, Inc., Natick, MA) for a global value of a manually drawn region of interest (ROI), and for each pixel within the same ROI, wherein the magnetisation M$_z$ is a function of the inversion time (TI), according to: $M_z(TI) = A - B\exp(-TI/C)$; with

$A = M_0(T_1^*/T_1)$; $B = M_0(1 + T_1^*/T_1)$; and $C = T_1^*$, and then $T_1 = (B/A - 1)T_1^*$. The difference between R$_1$ (=1/T$_1$) during carbogen and air breathing for each pixel was calculated and represented as oxygenation maps.

2.6. *Statistical analysis*

For the *in vivo* pO$_2$ measurements, one-tailed Wilcoxon tests were used to compare the mean changes between groups (air *vs.* carbogen breathing within the intramuscular, fibrosarcoma and glioblastoma groups). Histogram distributions, linear fits and Wilcoxon rank tests (for pixel-to-pixel analyses) with p values < 0.05 (*) were considered significant, and were calculated using Prism 5 software.

3. **Results**

3.1. *LNC preparation and characterisation*

The phase inversion process was exploited to obtain LNCs consisting of a lipidic-core (*i.e.* Labrafac) enclosed within a polymer-based (*i.e.* PEG) shell. After osmolarity adjustment, the LNCs had an average size and PDI of 60.7 ± 0.9 nm and 0.152 ± 0.016, respectively. These physicochemical properties are comparable to previously studied LNCs for up to a year [21–23].

3.2. *In vitro validation of LNCs sensitivity to oxygen*

To assess the ability and sensitivity of the LNCs to probe oxygenation variations *in vitro*, R$_1$ relaxation rates of the formulation's lipid component (*i.e.* Labrafac core) was assessed, in LNCs equilibrated in different oxygen environments (0%, 21% and 100%) at 37 °C. As shown in Fig. 1, the R$_1$ of the CH$_2$ backbone of Labrafac is sensitive to oxygen variation. This is demonstrated by the linear relationship between the change in oxygen from 0 to 100% and the concurrent increase of R$_1$ by 30% (R^2 = 0.9948).

3.3. *Intramuscular pO$_2$ measurements with LNCs*

Following an intramuscular bolus injection of 40 μL of LNCs, a set of T$_2$-weighted RARE images was acquired to produce an anatomical image (Fig. 2a), which was used to define the location wherein the LNCs were deposited. Fig. 2b presents the last image of the MOBILE set, and shows the lipid deposit. It should be noted that the bright areas of the MOBILE image in Fig. 2b corresponds to the lipid deposit as well as to the subcutaneous fat surrounding the muscle tissue, while the dark areas within the muscle are where no LNCs were introduced. The absence of signal in the muscle highlights that basal muscular lipid
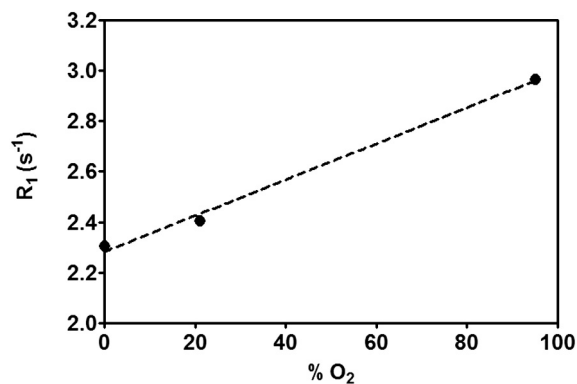

Fig. 1. *In vitro* sensitivity of the lipid relaxation rate (R$_1$) arising from lipid nanocapsules (LNCs) to oxygenation as measured by using the MOBILE MR sequence (R^2 = 0.9948).
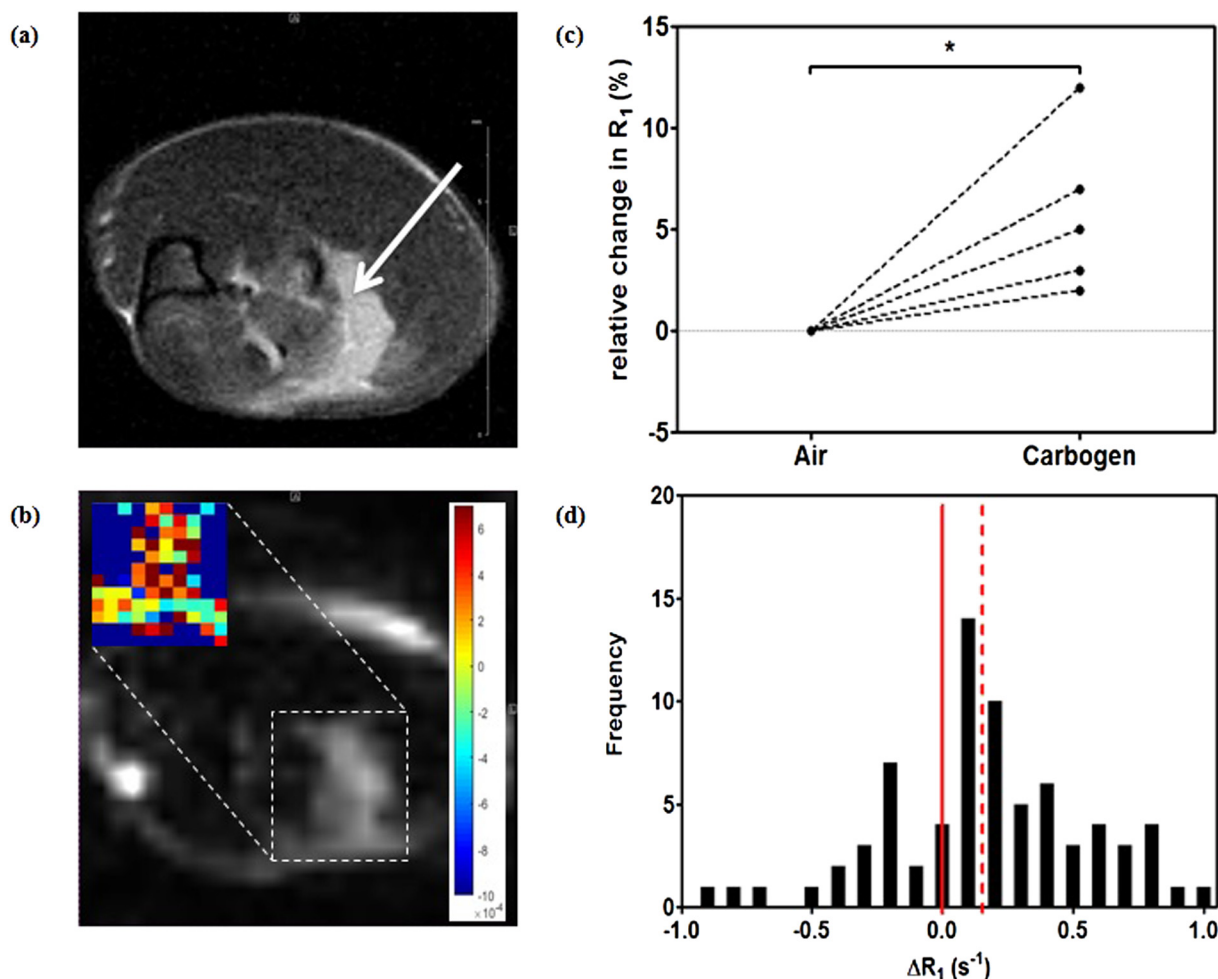
Fig. 2. Application of lipid nanocapsules (LNCs) to assess variations of oxygenation in the intramuscular tissue of mice using lipid relaxation rate measured with the MOBILE MR sequence, wherein (A) shows the transversal anatomical image of a mouse gastrocnemius muscle and the injected LNCs (indicated by arrow) and (B) shows the lipid image issued from the set of images acquired with the MOBILE MR sequence wherein the lipids from the LNCs can be observed. The global R_1 measured over the entire lipid deposit signal for all mice (n = 5) is shown in (C). The insert in (B) indicates the change in R_1 ($\Delta R_1 = R_{1\ carbogen} - R_{1\ air}$) for each pixel of lipid signal in the MOBILE image and a colour scale highlights the more responsive pixels in red (s^{-1}). ΔR_1 distribution of all encompassing pixels in the lipid deposit region of interest is represented as a histogram (D), wherein the median change of R_1 is indicated with a dotted red line.

content is too low to give rise to significant lipid signal. A ROI was drawn around the lipid hypersignal arising from the LNCs, and was used to calculate the global R_1 for each animal during air or carbogen breathing. Herein, the carbogen challenge was used to induce a transient increase in oxygenation within the normal and tumoural tissue, as previously demonstrated [7,24–26]. In the present study, an increase in oxygenation was observed through the increase in the global R_1 over the LNC area for all explored mice (Fig. 2c: p = 0.0313, n = 5) with an overall 6% mean increase. Moreover, a pixel-to-pixel analysis of the LNC area was also performed. The insert in Fig. 2b shows the R_1 change in the lipid deposit area induced by the carbogen challenge on a pixel-to-pixel basis with the corresponding ΔR_1 distribution histogram shown in Fig. 2d. For all mice, a median of 61% of pixels responded to the carbogen challenge and showed an increase in R_1. For the mouse presented in Fig. 2d, the median change in R_1 after the carbogen challenge was calculated at $0.1509\,s^{-1}$ with 66% of the pixels responding (for all mice = median change of $0.3450\,s^{-1}$). For data regarding all individuals in the intramuscular study, see the Supplementary documentation (S1).

3.4. Intratumoural pO$_2$ measurements with LNCs

Two tumoural models; the subcutaneous fibrosarcoma and the

intracerebral glioblastoma models were used in this study. These tumoural models were chosen to represent two types of severely hypoxic tissues (pO$_2$ < 10 mm Hg [26,27]) and their associated heterogeneity, as well as two different conditions in which LNCs could be administered into tumours. On the one hand, the subcutaneous fibrosarcoma tumours which are easily accessible and in which a bolus injection of LNC solution was deposited; and on the other hand, the intracerebral glioblastoma tumours in which the LNC solution was infused into the tumoural tissue using CED [19,20].

For the subcutaneous fibrosarcoma model, a bolus injection was performed similarly to the intramuscular model. To verify the correct targeting of the injection, a T$_2$-weighted anatomical RARE image set was performed (Fig. 3a), followed by the MOBILE sequence (Fig. 3b). As with the intramuscular experiments, a ROI was drawn around the lipid LNC signal in the last image of the MOBILE image set, and was used to determine the global R_1 change after the carbogen challenge for all the animals. A significant global R_1 variation for subcutaneous tumours was induced by the carbogen challenge (Fig. 3c; p = 0.0452, n = 7) with a 3% mean change for the responding animals (6 out of 7). To evaluate the response to the carbogen challenge more in depth, pixel-to-pixel R_1 variation maps illustrating the change in oxygenation was calculated, and an individual's response is illustrated in Fig. 3b & d. For all mice, a median of 71% of pixels responded to the carbogen challenge and was
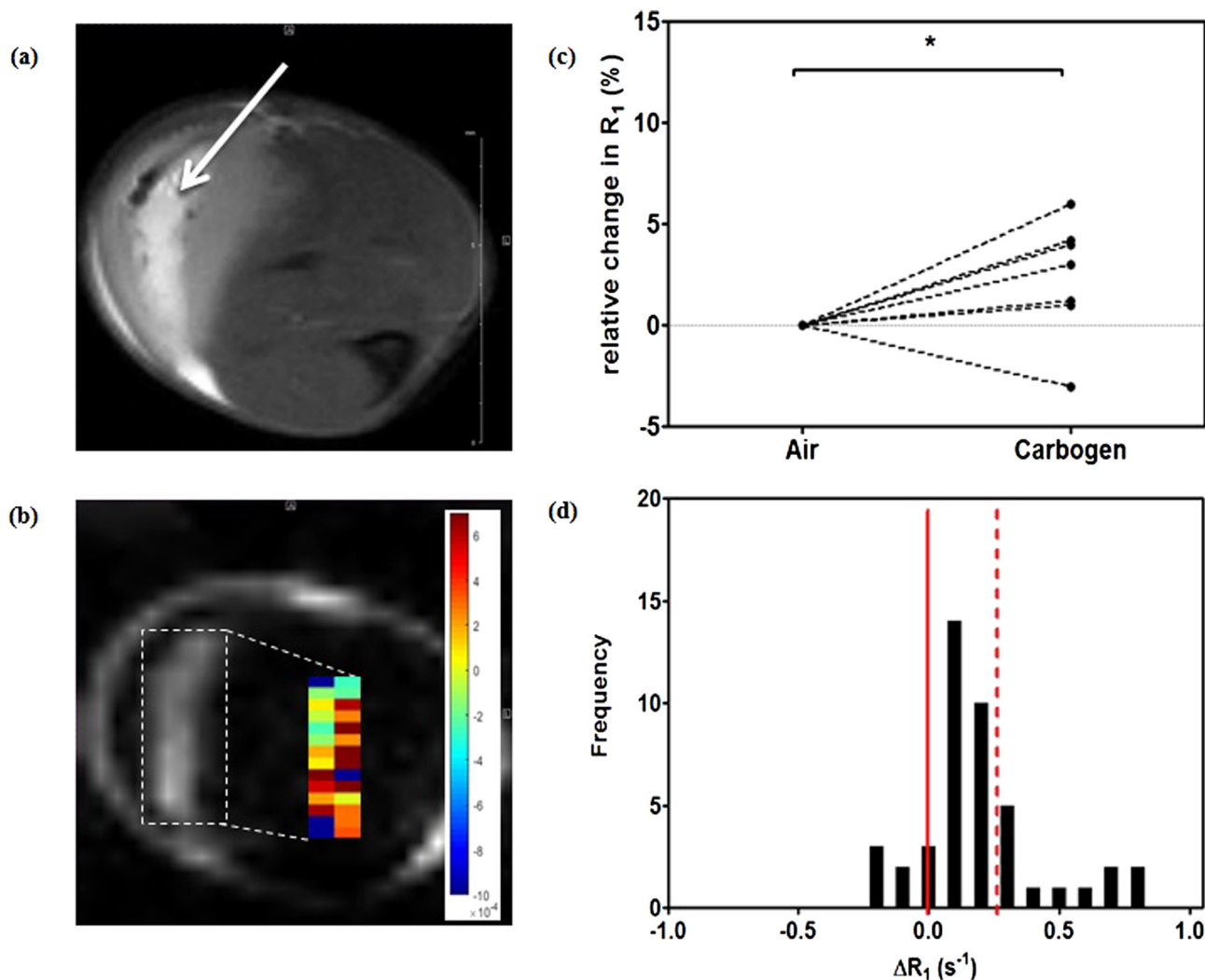
Fig. 3. Application of lipid nanocapsules (LNCs) to assess variations of oxygenation in a subcutaneous FSaII fibrosarcoma tumour mouse model using lipid relaxation rate measured with the MOBILE MR sequence, wherein (A) shows the transversal anatomical image of a fibrosarcoma tumour and the injected LNCs (indicated by arrow) and (B) shows the lipid image issued from the set of images acquired with the MOBILE MR sequence wherein the lipids from the LNCs can be observed. The global R_1 measured over the entire lipid deposit signal for all mice (n = 7) is shown in (C). The insert in (B) indicates the change in R_1 ($\Delta R_1 = R_{1\ carbogen} - R_{1\ air}$) for each pixel of lipid signal in the MOBILE image and a colour scale highlights the more responsive pixels in red (s^{-1}). ΔR_1 distribution of all encompassing pixels in the lipid deposit region of interest is represented as a histogram (D), wherein the median change of R_1 is indicated with a dotted red line.

associated with an increase in R_1. For the individual in Fig. 3b & d, the median change in R_1 after the carbogen challenge was calculated at 0.2034 s^{-1} with 71% of the pixels responding (for all mice = median change of 0.1779 s^{-1}). Data regarding all individuals in the subcutaneous fibrosarcoma tumour study are presented in the Supplementary documentation (S2).

For the intracerebral glioblastoma tumour model, a CED protocol was used to introduce the LNCs into the brain tumour and the distribution of the solution is apparent in the T_2-weighted anatomical RARE image (Fig. 4a). As in the two previous animal models, the MOBILE MR image (Fig. 4b) was used to draw the global ROI to determine the change in R_1. Here, a similar pattern emerges as with the subcutaneous fibrosarcoma tumours; five out of the six intracerebral glioblastoma tumours responded with an average of 6% increase in global R_1 (Fig. 4c; p = 0.0313, n = 6). Pixel-to-pixel analysis of the change in global R_1 from air to carbogen (Fig. 4b insert) highlights the response of an individual responding to the carbogen challenge, and all individuals in the intracerebral glioblastoma study are represented in the Supplementary documentation (S3). In the intracerebral glioblastoma study, a median of 62% of pixels for all animals responded to the carbogen challenge. For the individual in Fig. 4d, 76% of pixels

responded to the carbogen challenge to produce a median change of 0.2475 s^{-1} (median change of 0.3187 s^{-1} for all rats). It should also be noted, that for both the subcutaneous and glioblastoma models the MOBILE MR sequence was performed over the entire organ or leg. Thus, notwithstanding the bright area attributed to subcutaneous fat, other tissues appear as dark areas in the image sets (Figs. 3b & 4b) and illustrate that the intrinsic lipid content was not high enough to be detected, demonstrating the necessary input of lipid provided by the LNCs.

4. Discussion

In the present work, the main objective was to demonstrate the ability of LNCs to probe the oxygen level of normal and tumoural tissues. This was achieved using the MOBILE MR sequence [10] that was developed to assess oxygenation based on lipid longitudinal relaxation time. LNCs are excellent for use in tumour therapeutics as they are size tuneable, can avoid the immune system, have a neutral surface charge, are formulated with FDA approved constituents which make them suitable for *in vivo* administration, and they possess a large lipidic reservoir in which lipophilic agents and drugs can be embedded [28,29].
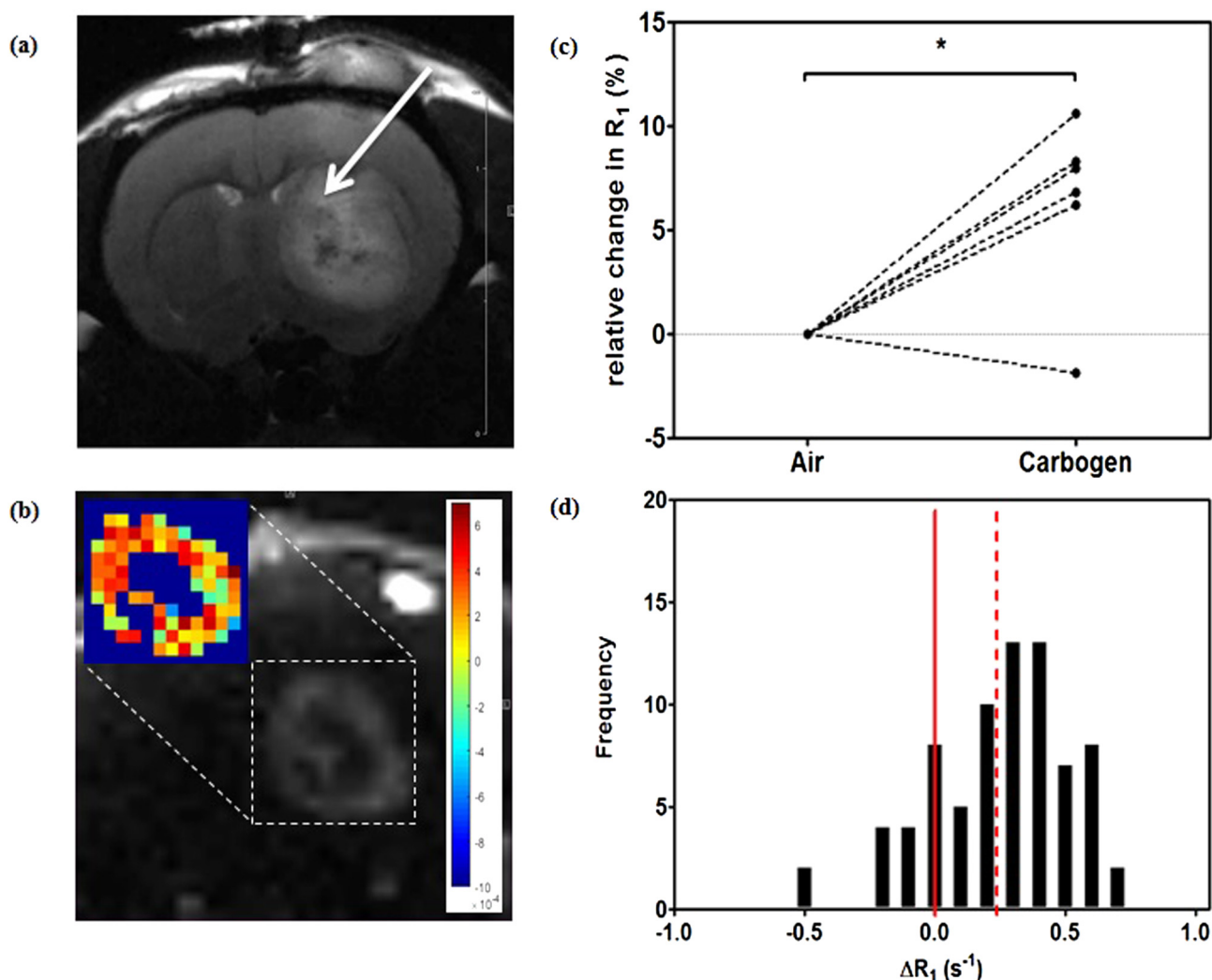
Fig. 4. Application of lipid nanocapsules (LNCs) to assess variations of oxygenation in a glioblastoma tumour rat model using lipid relaxation rate measured with the MOBILE MR sequence, wherein (A) shows the transversal anatomical image of a glioblastoma tumour and the injected LNCs (indicated by arrow) and (B) shows the lipid image issued from the set of images acquired with the MOBILE MR sequence wherein the lipids from the LNCs can be observed. The global R_1 measured over the entire lipid deposit signal for all rats (n = 6) is shown in (C). The insert in (B) indicates the change in R_1 ($\Delta R_1 = R_{1\ carbogen} - R_{1\ air}$) for each pixel of lipid signal in the MOBILE image and a colour scale highlights the more responsive pixels in red (s^{-1}). ΔR_1 distribution of all encompassing pixels in the lipid deposit region of interest is represented as a histogram (D), wherein the median change of R_1 is indicated with a dotted red line.

Thus LNCs, which are already used as a therapeutic nanocarrier [13,28–31], could also provide oxygenation information of tissues and double as a diagnostic tool thus becoming a theranostic platform. The ability of LNCs to respond to variations in oxygen was established using *in vitro* conditions wherein the oxygenation environment was controlled. Oxygen level variation accounts for a substantial change in R_1 and a linear relationship could be established (Fig. 1); as oxygenation increased, R_1 increased correspondingly. This relationship between the R_1 of lipids found in the LNCs and oxygen content could be reliably demonstrated and led to *in vivo* experimentation.

Thus, to further test the ability of the LNCs to probe oxygenation variation *in vivo*, a carbogen challenge was performed using three animal tissue models, namely a normal gastrocnemius muscle tissue model and two tumoural tissue models [32–35]. A bolus injection was used to introduce the LNC formulation into the muscle tissue, and the MOBILE MR image after the injection showed that the solution remained as a conglomeration, *i.e.* as a 'drop' (Figs. 2 & 3b). This 'drop' of injected LNCs remained as is for the duration of the experiments and did not diffuse throughout the tissue. This can be attributed to the direct injection into the tissue; since the LNCs circumvent the washout and biodistribution associated with an intravenous injection [36–39]

this allows for the formulation's sustained presence within the tissue. Thus, the persistence of a 'drop' of injected LNCs within the tissue is to be expected, as the normal gastrocnemius muscle is a highly hierarchized tissue and the bolus injection takes place over a short period of time, thus not allowing the liquid to disperse throughout the tissue. Regardless of the dispersion of the injected LNCs in the tissue, the lipids in the LNCs responded to the carbogen challenge and a map portraying the variation of the T_1 relaxation rate induced by percentage O_2 inhaled could be produced. This map enabled the visualisation of tissue pO_2 of the normal gastrocnemius muscle. Of note, the intrinsic muscular lipidic signal is too low to portray the effect of the challenge, thus making the LNC injection compulsory as no lipid signal can be observed outside the lipid drop (Fig. 2b). This observation was also noted in the tumoural models used in this study (Figs. 3 & 4b).

Within the subcutaneous fibrosarcoma tumours, an overall more limited response to the carbogen challenge was noted; an average R_1 increase of 3%, as compared to the 6% from both the gastrocnemius muscles and intracerebral glioblastomas (Figs. 2–4c). This muted response could be attributed to the poor blood perfusion prevalent in this tumour model [27,40,41], which limits the blood's transportation of the carbogen gas to the tissue environment near the drop of LNCs.

Similarly, this could explain the instance in which the R_1 decreased after the carbogen challenge in an individual animal. On the contrary, the intracerebral glioblastoma model, is associated with a heterogeneous tumour microenvironment which is highly vascularised [26]. This readily explains the increased response of this tumour model, comparative to the normal gastrocnemius muscle tissue, to the carbogen challenge. Furthermore, the methods of LNC introduction between the two tumour models should be noted. The CED protocol allowed for a more even distribution of the LNCs throughout the brain tumour tissue, whereas the bolus injection within the muscle and subcutaneous tumour model only allowed for the mapping of the LNCs within the drop.

Oxygenation mapping within the normal tissue and tumoural models showed that LNCs were able to improve the lipid signal-to-noise ratio to such an extent that pixel-to-pixel analysis of the area was achievable. Therefore, it was possible to image and analyse the response of each pixel to the carbogen challenge within all the animal models without using ionising probes or specialised ^{19}F-based MR equipment [15,42], thus making our system more widely applicable. Furthermore, in our study, the bolus injection allowed for a very specific site within the muscle and subcutaneous fibrosarcoma tumour to be analysed, whereas the CED diffusion of the LNCs throughout the intracerebral glioblastoma model allowed for the mapping and analysis of the entire area of the injected LNCs. Using the pixel-to-pixel analysis, it was possible to map the heterogeneity of the response from air to carbogen breathing for each animal (Figs. 2–4c) and the median overall change of the pixels could be calculated (Figs. 2–4d).

Although mapping of pO_2 change in tissue was achievable and successful, the conversion of R_1 to pO_2 proved difficult *in vivo*. Direct conversion, on the basis of data presented in Fig. 1, of R_1 into absolute pO_2 values cannot be done because although R_1 has been shown to be dependent on oxygenation it is also dependant on the heterogeneity of tissues, viscosity and iron content for example [43–46], all of which are variables that cannot be easily mimicked *in vitro*.

5. Conclusion

Herein, our aim was to demonstrate that LNCs, besides its proved therapeutic nanocarrier efficiency, could be used as a diagnostic tool in the form of an oxygen sensor for normal and tumoural tissue using the MOBILE MR sequence. LNCs were synthesised using the phase-inversion process, and the osmolarity of the formulation was adjusted for safe *in vivo* use. *In vitro* validation showed a linear relationship between oxygen variation and R_1, thus demonstrating the permeability and responsiveness of the LNCs to oxygen. For *in vivo* experimentation, three animal models; a normal muscle model and two tumoural tissue models (subcutaneous fibrosarcoma and intracerebral glioblastoma), were subjected to a carbogen challenge (95% O_2, 5% CO_2) to induce transient oxygenation changes within the tissue. From a single bolus injection of the LNCs, both a global R_1 value, as well as a pixel-to-pixel analysis was possible, due to the improved signal-to-noise provided by the lipid-core of the LNCs. However, because the bolus injection occurred over a short period of time, a limited area of tissue could be mapped. Thus, a CED injection was used to diffuse the LNCs throughout the intracerebral glioblastoma tumours to provide a more detailed oxygenation and heterogeneity map. Unfortunately, only relative pO_2 values were achievable from the LNC system as a myriad of parameters influence T_1 relaxation *in vivo*. Regardless, these developments and results indicate that LNCs could be used as both a therapeutic and diagnostic tool for cancer.

Acknowledgements

Conflict of interest

The authors report no conflict of interest.

Appendix A. Supplementary data

Supplementary data to this article can be found online at https://doi.org/10.1016/j.msec.2019.03.104.

References

[1] P. Vaupel, L. Harrison, Tumor hypoxia: causative factors, compensatory mechanisms, and cellular response, Oncologist 9 (Suppl. 5) (2004) 4–9, https://doi.org/10.1634/theoncologist.9-90005-4.

[2] S. Ramachandran, J. Ient, E.-L. Göttgens, A. Krieg, E. Hammond, Epigenetic therapy for solid tumors: highlighting the impact of tumor hypoxia, Genes (Basel) 6 (2015) 935–956, https://doi.org/10.3390/GENES6040935.

[3] J.G. Riess, M. Le Blanc, Perfluoro compounds as blood substitutes, Angew. Chem. Int. Ed. Engl. 17 (1978) 621–634, https://doi.org/10.1002/anie.197806213.

[4] P. Parhami, B.M. Fung, Fluorine-19 relaxation study of perfluoro chemicals as oxygen carriers, J. Phys. Chem. 87 (1983) 1928–1931, https://doi.org/10.1021/j100234a020.

[5] J. Ruiz-Cabello, B.P. Barnett, P.A. Bottomley, J.W.M.M. Bulte, Fluorine (19F) MRS and MRI in biomedicine, NMR Biomed. 24 (2011) 114–129, https://doi.org/10.1002/nbm.1570.

[6] R.B. Lauffer, Paramagnetic metal complexes as water proton relaxation agents for NMR imaging: theory and design, Chem. Rev. 87 (1987) 901–927, https://doi.org/10.1021/cr00081a003.

[7] J.P.B. O'Connor, A. Jackson, G.A. Buonaccorsi, D.L. Buckley, C. Roberts, Y. Watson, S. Cheung, D.M. McGrath, J.H. Naish, C.J. Rose, P.M. Dark, G.C. Jayson, G.J.M. Parker, Organ-specific effects of oxygen and carbogen gas inhalation on tissue longitudinal relaxation times, Magn. Reson. Med. 58 (2007) 490–496, https://doi.org/10.1002/mrm.21357.

[8] C.H. Sotak, P.S. Hees, H.-N. Huang, M.-H. Hung, C.G. Krespan, S. Raynolds, A new perfluorocarbon for use in fluorine-19 magnetic resonance imaging and spectroscopy, Magn. Reson. Med. 29 (1993) 188–195, https://doi.org/10.1002/mrm.1910290206.

[9] H.F. Bennett, H.M. Swartz, R.D. Brown, S.H. Koenig, Modification of relaxation of lipid protons by molecular oxygen and nitroxides, Investig. Radiol. 22 (1987) 502–507 http://www.ncbi.nlm.nih.gov/pubmed/3040617.

[10] B.F. Jordan, J. Magat, F. Colliez, E. Ozel, A.C. Fruytier, V. Marchand, L. Mignion, C. Bouzin, P.D. Cani, C. Vandeputte, O. Feron, N. Delzenne, U. Himmelreich, V. Denolin, T. Duprez, B. Gallez, Mapping of oxygen by imaging lipids relaxation enhancement: a potential sensitive endogenous MRI contrast to map variations in tissue oxygenation, Magn. Reson. Med. 70 (2013) 732–744, https://doi.org/10.1002/mrm.24511.

[11] B. Heurtault, P. Saulnier, B. Pech, J.-E. Proust, J.-P. Benoit, A novel phase inversion-based process for the preparation of lipid nanocarriers, Pharm. Res. 19 (2002) 875–880, https://doi.org/10.1023/A:1016121319668.

[12] N.T. Huynh, C. Passirani, E. Allard-Vannier, L. Lemaire, J. Roux, E. Garcion, A. Vessieres, J. Benoit, Administration-dependent efficacy of ferrociphenol lipid nanocapsules for the treatment of intracranial 9L rat gliosarcoma, Int. J. Pharm. 423 (2012) 55–62, https://doi.org/10.1016/j.ijpharm.2011.04.037.

[13] C. Bastiancich, K. Vanvarenberg, B. Ucakar, M. Pitorre, G. Bastiat, F. Lagarce, V. Préat, F. Danhier, Lauroyl-gemcitabine-loaded lipid nanocapsule hydrogel for the treatment of glioblastoma, J. Control. Release 225 (2016) 283–293, https://doi.org/10.1016/J.JCONREL.2016.01.054.

[14] C. Vanpouille-Box, F. Lacoeuille, C. Belloche, N. Lepareur, L. Lemaire, J.J. LeJeune, J.P. Benoit, P. Menei, O.F. Couturier, E. Garcion, F. Hindré, Tumor eradication in rat glioma and bypass of immunosuppressive barriers using internal radiation with (188)Re-lipid nanocapsules, Biomaterials 32 (2011) 6781–6790, https://doi.org/10.1016/j.biomaterials.2011.05.067.

[15] L. Lemaire, G. Bastiat, F. Franconi, N. Lautram, T. Duong Thi Dan, E. Garcion, P. Saulnier, J.P. Benoit, Perfluorocarbon-loaded lipid nanocapsules as oxygen sensors for tumor tissue pO2 assessment, Eur. J. Pharm. Biopharm. 84 (2013) 479–486, https://doi.org/10.1016/j.ejpb.2013.01.003.

[16] A. Vonarbourg, C. Passirani, P. Saulnier, P. Simard, J.C. Leroux, J.-P. Benoit, Evaluation of pegylated lipid nanocapsules versus complement system activation and macrophage uptake, Wiley Period. 78 (2006) 620–628. doi:https://doi.org/10.1002/jbm.a.

[17] J.P. Volpe, N. Hunter, I. Basic, L. Milas, Metastatic properties of murine sarcomas and carcinomas I. Positive correlation with lung colonization and lack of correlation with s.c. tumor take, Clin. Exp. Metastasis 3 (1985) 281–294, https://doi.org/10.1007/BF01585082.

[18] L. Lemaire, F. Franconi, J.P. Saint-André, V.-G. Roullin, P. Jallet, J.-J. Le Jeune, High-field quantitative transverse relaxation time, magnetization transfer and apparent water diffusion in experimental rat brain tumour, NMR Biomed. 13 (2000) 116–123, https://doi.org/10.1002/1099-1492(200005)13:3<116::AID-NBM616>3.0.CO;2-D.

[19] R.H. Bobo, D.W. Laske, A. Akbasak, P.F. Morrison, R.L. Dedrick, E.H. Oldfield,

Convection-enhanced delivery of macromolecules in the brain, Proc. Natl. Acad. Sci. U. S. A. 91 (1994) 2076–2080, https://doi.org/10.1073/PNAS.91.6.2076.

[20] E. Allard, C. Passirani, J.-P. Benoit, Convection-enhanced delivery of nanocarriers for the treatment of brain tumors, Biomaterials 30 (2009) 2302–2318, https://doi.org/10.1016/j.biomaterials.2009.01.003.

[21] B. Heurtault, P. Saulnier, B. Pech, J.-P. Benoit, J.-E. Proust, Interfacial stability of lipid nanocapsules, Colloids Surf. B Biointerfaces 30 (2003) 225–235, https://doi.org/10.1016/S0927-7765(03)00096-1.

[22] O. Thomas, F. Lagarce, Lipid nanocapsules: a nanocarrier suitable for scale-up process, J. Drug Delivery Sci. Technol. 23 (2013) 555–559, https://doi.org/10.1016/S1773-2247(13)50084-0.

[23] N. Anton, P. Gayet, J.-P. Benoit, P. Saulnier, Nano-emulsions and nanocapsules by the PIT method: an investigation on the role of the temperature cycling on the emulsion phase inversion, Int. J. Pharm. 344 (2007) 44–52, https://doi.org/10.1016/J.IJPHARM.2007.04.027.

[24] S.P. Robinson, F.A. Howe, J.R. Griffiths, Noninvasive monitoring of carbogen-induced changes in tumor blood flow and oxygenation by functional magnetic resonance imaging, Int. J. Radiat. Oncol. Biol. Phys. 33 (1995) 855–859, https://doi.org/10.1016/0360-3016(95)00072-1.

[25] G.S. Karczmar, V.Y. Kuperman, J.N. River, M.Z. Lewis, M.J. Lipton, Magnetic resonance measurement of response to hyperoxia differentiates tumors from normal tissue and may be sensitive to oxygen consumption, Investig. Radiol. 29 (1994) S161–S163 http://www.ncbi.nlm.nih.gov/pubmed/7928217.

[26] S. Valable, B. Lemasson, R. Farion, M. Beaumont, C. Segebarth, C. Remy, E.L. Barbier, Assessment of blood volume, vessel size, and the expression of angiogenic factors in two rat glioma models: a longitudinal in vivo and ex vivo study, NMR Biomed. 21 (2008) 1043–1056, https://doi.org/10.1002/nbm.1278.

[27] R. Ansiaux, C. Baudelet, B.F. Jordan, N. Beghein, P. Sonveaux, J. De Wever, P. Martinive, V. Grégoire, O. Feron, B. Gallez, Thalidomide radiosensitizes tumors through early changes in the tumor microenvironment, Clin. Cancer Res. 11 (2005) 743–750 http://www.ncbi.nlm.nih.gov/pubmed/15701864.

[28] G. Lollo, M. Vincent, G. Ullio-Gamboa, L. Lemaire, F. Franconi, D. Couez, J.-P. Benoit, Development of multifunctional lipid nanocapsules for the co-delivery of paclitaxel and CpG-ODN in the treatment of glioblastoma, Int. J. Pharm. 495 (2015) 972–980, https://doi.org/10.1016/j.ijpharm.2015.09.062.

[29] C. Bastianich, L. Lemaire, J. Bianco, F. Franconi, F. Danhier, V. Préat, G. Bastiat, F. Lagarce, Evaluation of lauroyl-gemcitabine-loaded hydrogel efficacy in glioblastoma rat models, Nanomedicine 13 (2018) 1999–2013, https://doi.org/10.2217/nnm-2018-0057.

[30] N.T. Huynh, C. Passirani, P. Saulnier, J.P. Benoit, Lipid nanocapsules: a new platform for nanomedicine, Int. J. Pharm. 379 (2009) 201–209, https://doi.org/10.1016/J.IJPHARM.2009.04.026.

[31] A. Clavreul, N. Lautram, F. Franconi, C. Passirani, C. Montero-Menei, P. Menei, C. Tetaud, A. Montagu, A.-L. Laine, A. Vessieres, Targeting and treatment of glioblastomas with human mesenchymal stem cells carrying ferrociphenol lipid nanocapsules, Int. J. Nanomedicine 10 (2015) 1259–1271, https://doi.org/10.2147/IJN.S69175.

[32] J.A. Kruuv, W.R. Inch, J.A. McCredie, Blood flow and oxygenation of tumors in mice. I. Effects of breathing gases containing carbon dioxide at atmospheric pressure, Cancer 20 (1967) 51–59 http://www.ncbi.nlm.nih.gov/pubmed/6016872.

[33] D.W. Siemann, R.P. Hill, R.S. Bush, The importance of the pre-irradiation breathing times of oxygen and carbogen (5% CO2: 95% O2) on the in vivo radiation response

of a murine sarcoma, Int. J. Radiat. Oncol. Biol. Phys. 2 (1977) 903–911, https://doi.org/10.1016/0360-3016(77)90188-2.

[34] J.L. Lanzen, R.D. Braun, A.L. Ong, M.W. Dewhirst, Variability in blood flow and pO2 in tumors in response to carbogen breathing, Int. J. Radiat. Oncol. Biol. Phys. 42 (1998) 855–859, https://doi.org/10.1016/S0360-3016(98)00312-5.

[35] N. Khan, H. Li, H. Hou, J.P. Lariviere, D.J. Gladstone, E. Demidenko, H.M. Swartz, Tissue pO2 of orthotopic 9L and C6 gliomas and tumor-specific response to radiotherapy and hyperoxygenation, Int. J. Radiat. Oncol. Biol. Phys. 73 (2009) 878–885, https://doi.org/10.1016/j.ijrobp.2008.10.025.

[36] M.N. Khalid, P. Simard, D. Hoarau, A. Dragomir, J.-C. Leroux, Long circulating poly (ethylene glycol)-decorated lipid nanocapsules deliver docetaxel to solid tumors, Pharm. Res. 23 (2006) 752–758, https://doi.org/10.1007/s11095-006-9662-5.

[37] S. Ballot, N. Noiret, F. Hindré, B. Denizot, E. Garin, H. Rajerison, J.-P. Benoit, 99mTc/188Re-labelled lipid nanocapsules as promising radiotracers for imaging and therapy: formulation and biodistribution, Eur. J. Nucl. Med. Mol. Imaging 33 (2006) 602–607, https://doi.org/10.1007/s00259-005-0007-0.

[38] F. Lacoeuille, F. Hindre, F. Moal, J. Roux, C. Passirani, O. Couturier, P. Cales, J.J. Le Jeune, A. Lamprecht, J.P. Benoit, In vivo evaluation of lipid nanocapsules as a promising colloidal carrier for paclitaxel, Int. J. Pharm. 344 (2007) 143–149, https://doi.org/10.1016/J.IJPHARM.2007.06.014.

[39] A. Cahouet, B. Denizot, F. Hindré, C. Passirani, B. Heurtault, M. Moreau, J. Le Jeune, J. Benoît, Biodistribution of dual radiolabeled lipidic nanocapsules in the rat using scintigraphy and γ counting, Int. J. Pharm. 242 (2002) 367–371, https://doi.org/10.1016/S0378-5173(02)00218-1.

[40] B.F. Jordan, N. Beghein, M. Aubry, V. Grégoire, B. Gallez, Potentiation of radiation-induced regrowth delay by isosorbide dinitrate in FSaII murine tumors, Int. J. Cancer 103 (2003) 138–141, https://doi.org/10.1002/ijc.10786.

[41] B.F. Jordan, V. Grégoire, R.J. Demeure, P. Sonveaux, O. Feron, J. O'Hara, V.P. Vanhulle, N. Delzenne, B. Gallez, Insulin increases the sensitivity of tumors to irradiation: involvement of an increase in tumor oxygenation mediated by a nitric oxide-dependent decrease of the tumor cells oxygen consumption, Cancer Res. 62 (2002) 3555–3561 http://www.ncbi.nlm.nih.gov/pubmed/12068004.

[42] P. Zanzonico, J. O'Donoghue, J.D. Chapman, R. Schneider, S. Cai, S. Larson, B. Wen, Y. Chen, R. Finn, S. Ruan, L. Gerweck, J. Humm, C. Ling, J. O'Donoghue, J.D. Chapman, R. Schneider, S. Cai, S. Larson, B. Wen, Y. Chen, R. Finn, S. Ruan, L. Gerweck, J. Humm, C. Ling, Iodine-124-labeled iodo-azomycin-galactoside imaging of tumor hypoxia in mice with serial microPET scanning, Eur. J. Nucl. Med. Mol. Imaging 31 (2004) 117–128, https://doi.org/10.1007/s00259-003-1322-y.

[43] D. Hernando, S.D. Sharma, H. Kramer, S.B. Reeder, On the confounding effect of temperature on chemical shift-encoded fat quantification, Magn. Reson. Med. 72 (2014) 464–470, https://doi.org/10.1002/mrm.24951.

[44] C.L. Hoad, N. Palaniyappan, P. Kaye, Y. Chernova, M.W. James, C. Costigan, A. Austin, L. Marciani, P.A. Gowland, I.N. Guha, S.T. Francis, G.P. Aithal, A study of T1 relaxation time as a measure of liver fibrosis and the influence of confounding histological factors, NMR Biomed. 28 (2015) 706–714, https://doi.org/10.1002/nbm.3299.

[45] K.M. Donahue, R.M. Weisskoff, D. Burstein, Water diffusion and exchange as they influence contrast enhancement, J. Magn. Reson. Imaging 7 (1997) 102–110, https://doi.org/10.1002/jmri.1880070114.

[46] P. Kellman, M.S. Hansen, T1-mapping in the heart: accuracy and precision, J. Cardiovasc. Magn. Reson. 16 (2014) 1–20, https://doi.org/10.1186/1532-429X-16-2.